High current field emission from individual non-linear resistor ballasted carbon nanotube cluster array

Zhenjun Li [a], *Xiaoxia Yang* [a], *Feng He* [b], *Bing Bai* [a], *Hang Zhou* [b], *Chi Li* [a,*], *Qing Dai* [a,*]

[a] *National Center for Nanoscience & Technology, Beijing 100190, PR China*
[b] *School of Electronic and Computer Engineering, Peking University, Shenzhen, PR China*

A B S T R A C T

Field emission (FE) electron sources based on carbon nanotubes (CNTs) have the potential to serve as cold cathodes for various vacuum microelectronic and nanoelectronic devices. Emission currents are extremely sensitive to variation in emitter geometry and local surface states, both of which are difficult to synthesize uniformly when fabricating a CNT field emission array (FEA). Such non-uniformities cause unstable emission, limiting the current output. Here, we propose a method for simulating and fabricating a high performance CNT-FEA with emission units that are individually connected to a single crystalline silicon pillar (SP), which acts as an non-linear ballast resistor. Results showed that the driving field for this CNT-FEA was greatly reduced relative to CNT-FEAs on a flat silicon substrate. This improvement was due to the high aspect ratio of the CNT clusters combined with SPs. The FE behavior demonstrated that the emission current was limited by the non-linear resistors (NLRs). Emitted currents density over 1.65 A/cm^2 at a low extraction field of 5.8 V/μm were produced by a 1 mm^2 emmiting area. The proposed technology may be used to fabricate cathodes capable of reliable, uniform, and high current emission.

1. Introduction

Field emission (FE) electron sources have many potential applications, including flat panel displays [1], ion thrusters [2], X-ray sources [3,4], and microwave amplifiers [5]. In most of these applications, the current, stability, lifetime, and emission uniformity are the main determinants of cathode performance [3,4,6,7]. Although numerous materials may serve as an FE source, carbon nanotubes (CNTs) have attracted significant interest [8–10] because of their unique properties, such as high aspect ratio and small tip radius. However, thus far, field emitters array (FEA) based on CNTs have been seldom used in practice due to their limited ability to emit electrons. Although some emitters may produce a high current, the short lifetime of the emitters is problematic [11–16].

One of the key issues limiting CNT-FEA technology is difficulty to control the uniformity of CNT emitters' morphology. For instance, in a CNT-FEA, because of variation in local field enhancement affected by emitters' geometry and position, the total emission current contribution from each emitter will be different [9,17–19], which can be concluded from the Fowler–Nordheim (FN) theory [20–22]. When the applied field increases and the emission current from an individual

* *Corresponding authors.*
E-mail addresses: daiq@nanoctr.cn (Q. Dai), lichi@nanoctr.cn (C. Li).
http://dx.doi.org/10.1016/j.carbon.2015.03.018

emitter exceeds an intrinsic threshold value, irreversible changes will occur at the emitting tips, usually resulting in the destruction of the CNTs [23,24]. Consequently, the non-uniform emission in the CNT-FEA will cause an short lifetime and limit the total emission current.

To produce a large emission current, currents from many CNT emitters must be combined in an array. An effective method is to restrain the emission current from each emitter under the threshold value, which also protects them from destruction. A non-linear resistor (NLR) may achieve reasonable saturation current, which can be controlled in proportion to the threshold emission current. In previous work, we used an individual field effect transistor ballasted CNT array fabricated on a silicon-on-insulator (SOI) substrate to produce a very high current density [25]. However, the fabrication process was complex and expensive, and the CNT array appeared too fragile for practical applications. Here, we propose a systematic method, including an effective simulation and simplified fabrication, for constructing individual NLR ballasted CNT cluster FEAs with high FE performance.

As shown in Fig. 1, each CNT cluster emitter in the array are individually connected to a single crystalline silicon pillar (SP), which functions as a ballast NLR. As the emission current increases in response to an increasing applied field, the current passing the channel of the NLR eventually saturates, limiting the emission current. First, we investigated the threshold emission current of individual CNT clusters. Then, the SP array was designed to produce a saturation current lower than the threshold emission current and to diminish the screening effect between adjacent emitting units. Next, a simple method was developed to fabricate the hybrid structure. Finally, the field emission performance of the CNT–SP FEA was investigated.

2. Results and discussion

To measure the threshold current (*I*th, defined as the maximum stable emission current that CNT cluster can tolerate) of an individual CNT cluster, the CNT cluster array was first grown on a flat, heavily doped silicon substrate (sample S0) by chemical vapor deposition (CVD). A detailed growth process is described in the Section 4. Fig. S1(a) is a scanning electron microscopy (SEM) image of a CNT cluster array. To ensure vertical alignment, the height of a single cluster was fixed at 5 μm, and the diameter was fixed at 3 μm. If CNT clusters longer than 10 μm, they will be bended due to their low hardness, as shown in Fig. S1(b). A CNT cluster array with inferior alignment will have poor field emission properties. In contrast, a CNT cluster that is too short will have a low field enhancement factor. Thus, the SP array introduced in this work also function as the template for CNT cluster array to increase the field enhancement effect, as discussed below. The field emission properties of one hundred individual CNT clusters were tested using a nano-manipulator in a SEM, as described in the Section 4 and in Fig. S1(c and e). The obtained values of *I*th at different electric fields for all 100 clusters were recorded in Fig. S1(f), of which the lowest limit was 10 μA. Thus, the saturation current of an individual SPs should be less than 10 μA to protect the CNT clusters. The large sample size enabled the measurement of a reliable *I*th value which was able to represent the universal emitters in the array.

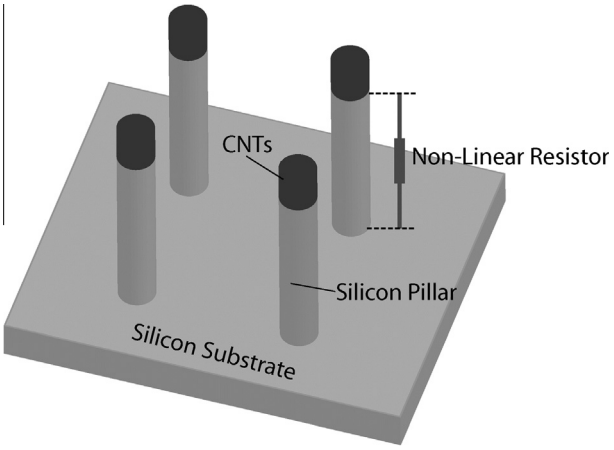

Fig. 1 – Schematic of SP NLR ballasted CNT cluster emitter array.

In a highly ordered FEA, the geometry of the array units must be designed to increase the field enhancement effect. In our experiments, the diameter and spacing of CNT–SP structures were fixed at 3 μm and 15 μm, respectively. To investigate the effect of the SP length on the electric field enhancement of the array, we performed a three-dimensional (3D) finite element electrostatic simulation employing COMSOL MULTIPHYSICS (see Supporting Information). To simplify the simulation, the heavily doped SPs were modeled as solid metal [26]. Twenty-five SP units were placed in a 5 V/μm electrostatic field. The top view of the electric field distribution around the SP structure is plotted in the inset of Fig. 2(a). Fig. 2 shows the effect of SP length on the normalized local electric field at a defined point (red arrow), as shown in the inset of Fig. 2. If the length of the SP is longer than 20 μm, the local electric field is not change any more, suggesting a fully enhanced local field. Thus, to guarantee a maximum field enhancement effect, the CNT–SP structure was fabricated to ~25 μm with ~2 μm CNT cluster and ~23 μm SP.

Then, we calculated the dependency of the doping concentration of the silicon chip needed for the SP fabrication on the saturation current of the SP NLR. In the simulation, the cross-sectional area of a single SP NLR was a circle with a diameter of 3 μm, and the channel length was 23 μm. Fig. 2(b) shows the saturation current as a function of the doping concentration (from 10^{11} to 10^{18} cm^{-3}) for the SP NLR, which was also simulated by COMSOL MULTIPHYSICS (see Supporting Information). A doping concentration of 5×10^{14} cm^{-3} is required for a saturation current of 8 μA, the current chosen for the SP array fabrication (sample S1). For comparison, silicon chips with a doping concentration of 2×10^{14} cm^{-3} (sample S2) and 2×10^{15} cm^{-3} (sample S3) were used to fabricate SP arrays, of which a single SP had a saturation current of 2 μA and 90 μA, respectively.

After determining the SP parameters, FEAs with a large area (4900 emitters in 1 mm^2) were fabricated to demonstrate high, uniform field emission currents. The fabrication process is shown in Fig. 3(a–d, e and f) shows the morphology of the

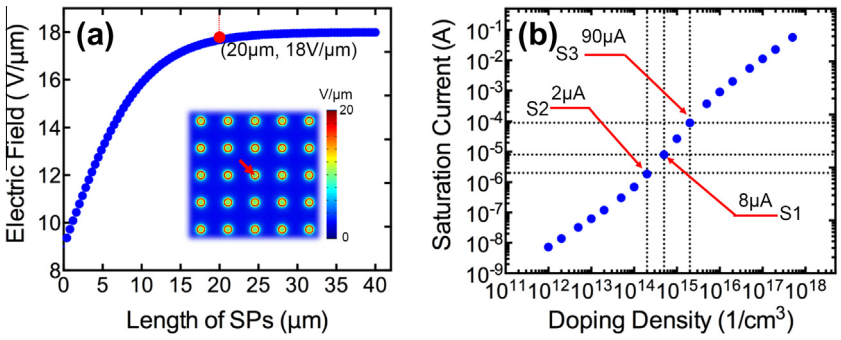

Fig. 2 – (a) The influence of SP length on the normalized local electric field at the defined point (red arrow) as shown in the inset, which suggested a optimized length of 20 μm. The inset shows the top view of the electric field distribution on the top SP structures. (b) The saturation current of a single SP NLR as a function of the doping concentration. The doping concentration of 5×10^{14}, 2×10^{14} and 2×10^{15} cm^{-3} were chosen, corresponding to a saturation current of 8 μA (S1), 2 μA (S2), and 90 μA (S3), respectively. (A color version of this figure can be viewed online.)

fabricated CNT–SP array under low and high magnification, respectively. The silicon substrates were first coated with an aluminum/iron bi-layer catalyst to facilitate CNT growth and then coated with a thick photo-resistor (PR) layer. These thin films were then patterned using contact photolithography and wet etching to form arrays of 70×70 dots with a 3 μm diameter and a spacing of 15 μm. Next, the vertical SP NLRs were etched using deep reaction ion etching (DRIE), and the top PR layer was cleaned. Finally, the CNT cluster array was grown on top of the SP array by CVD as described in the Section 4. A transmission electron micrograph (TEM) and Raman spectrum of the CNTs are shown in the Fig. S4(a) and (b), respectively, which demonstrate that the crystallinity and purity of the CNTs.

The SP NLR is formed from a channel with asymmetric contacts. The bottom contact is the silicon substrate, functioning an abundant source of electrons when connected to the negative terminal of a power supply through a ohmic contact. The top contact, which is located at the CNT/SP junction, has a contact area of less than 10^{-12} m^2. This top contact receives but cannot source electrons in response to transport through the channel. As the electron current increases, the potential at the top contact becomes positive, leading to 'pinch-off' current saturation. The NLR behavior of the SPs was tested using the nano-manipulator described previously. All contacts were assumed to be ohmic contacts. The current–voltage characteristics of the SPs in S1 and S2 are shown in Fig. 4(a), in which the error bars indicate the current difference from SP to SP. The saturation bias voltage (V_{bias}) is about 20 V, which produces a saturation current of ~5.6 μA (S1) and ~1.1 μA (S2). The difference between the experimental and simulation results was probably due to non-ideal contact and geometrical deviation of SPs.

The FE of individual CNT–SP emitters were also measured using the nano-manipulator. The mean current–field (*I–E*) curves of the CNT–SPs in S1 and S2 are shown in Fig. 4(b), in which the error bars indicate the difference in the driving field between emitters. The field emission performance of the CNT-silicon pillars varied, but all of the curves saturated at a similar emission current of ~5.6 μA for S1 and ~1.1 μA for S2. The emission current was well within the safe tolerances for the individual CNT clusters, suggesting that each CNT–SP may safely emit current below the SP saturation current. Therefore, the ballasting NLRs offered integrated protection for the CNT clusters.

The field emission performance was tested for the entire ballasted structure array. The experimental setup for the field emission measurements is described in the Section 4. Fig. 4(c) displays the *I–E* curves for S0, S1, S2, and S3. Because the saturation current was 5.6 μA for each CNT–SP in S1 and the array contained 4900 CNT–SPs, theoretically, the total current should have been ~27 mA. However, the emission current was measured to be unsaturated at 16.5 mA, probably due to the power limitation of the FE testing rig. For S2, a saturation current of 5.16 mA was measured, closely matching the theoretically value (5.39 mA). The small difference between the theoretical and experimental saturation current is probably due to the loss of CNT clusters or SPs during fabrication. Although a low turn-on field is obtained from S3, the total emission current was about 3.4 mA, which was lower than S1 and S2. The emission current of S3 became unstable above 1 mA mainly due to the destruction of prior emitted CNT clusters. Because the saturation current of the SPs in S3 was higher than the threshold current of the CNT cluster, the SPs were not able to function as protecting NLRs. As expected, the driving voltage was much higher for S0 than for the other samples due to the lower field enhancement of the short CNT cluster. The threshold emission current was also much lower for S0 than for the others. These experiments provide parameters for successfully designing a high performance CNT–SP FEA.

Fig. 4(d) shows the corresponding FN plots. Two different regions are observed in the curves for S1. The bottom region is the pure field emission current (FN regime), and the top region is the NLR-limited emission current. Compared with S1, the curve for S2 has an additional region that bends downward at the top, indicating current saturation. The curve for S3 also contains two regions, but the behavior of the top region suggests that the emission current was limited by the resistance of the CNT clusters and the contact resistance between CNT clusters and SPs, the sum of which is around several MΩ, rather than the resistance of the NLR. For S3, no

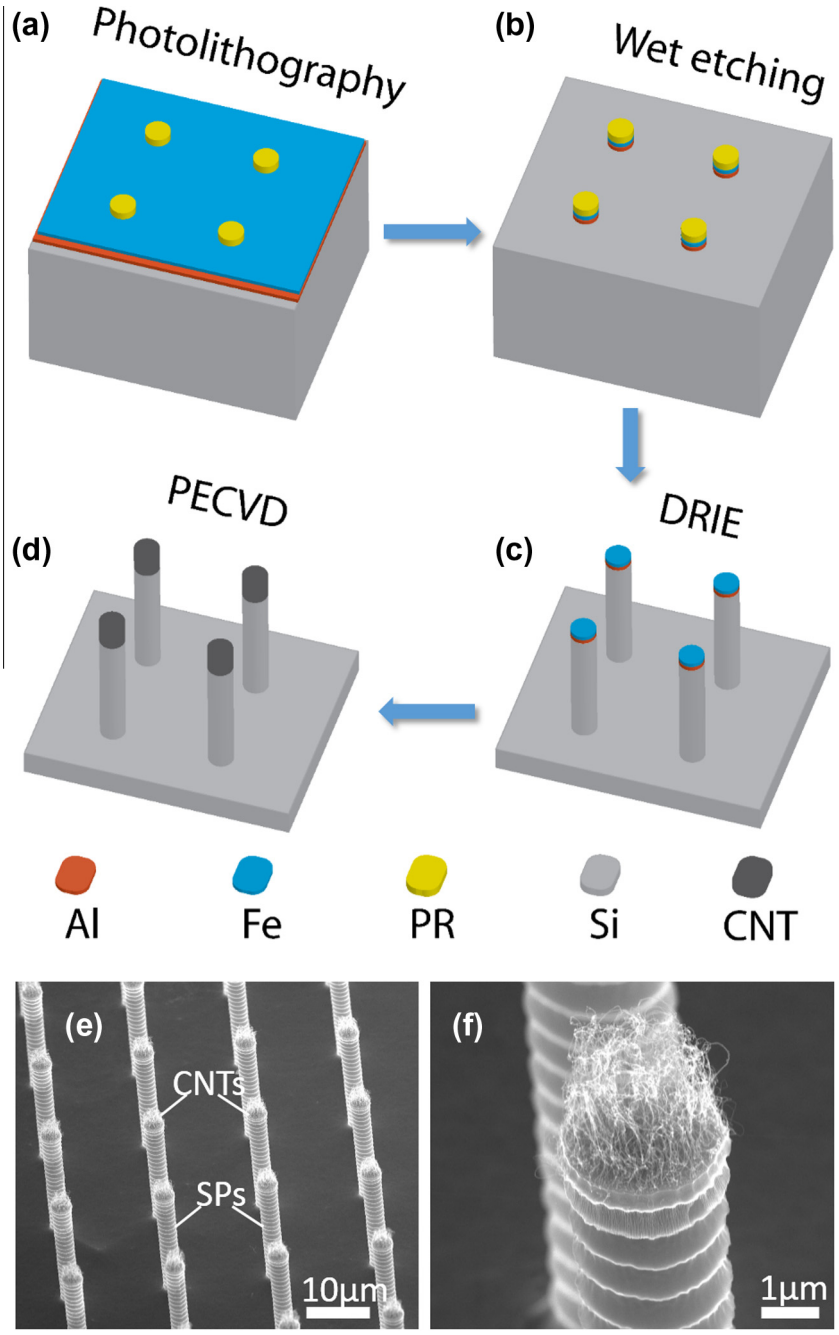

Fig. 3 – (a–d) Process flow to fabricate the CNT–SP FEA. (e) and (f) show the SEMs of as-fabricated CNT–SP array in low and high magnification, respectively. (A color version of this figure can be viewed online.)

resistance-limited emission was observed because the current was very low. The data in the FN regions were fitted using the FN equation, which is given below [27,28]:

$$J = A(\beta^2 E^2/\Phi)\exp(-B\Phi^{3/2}/\beta E),$$

where J is the emission current density (the total emission current divided by the effective emission area); $A = 1.56 \times 10^{-6}$ AV^{-2} eV; $B = 6.83 \times 10^{9}$ V $eV^{-3/2}$ Vm^{-1}; β is a field enhancement factor that is proportional to the aspect ratio of the electron emitter; Φ is the work function (4.8 eV for CNT); and E is the applied electric field. The regions of interest in the FN plots correspond to regions of interest in the I–E curves. The field enhancement factor of bare CNTs (β) may be calculated using the slope (S) of the linearized FN data in the formula:

$$S = -B\Phi^{3/2}/\beta.$$

The calculated β for S1 is 5600; S2 is 5230; S3 is 5840; and S0 is 1200. The trend agrees well with the simulation results.

The temporal emission measurements were carried under a relatively low vaccum of $\sim 10^{-4}$ Pa to investigate the tolerance of the samples. As shown in Fig. 5, the stability of the ballasted structure (S1) was much higher than the unballasted structure (S3). The improved emission stability may

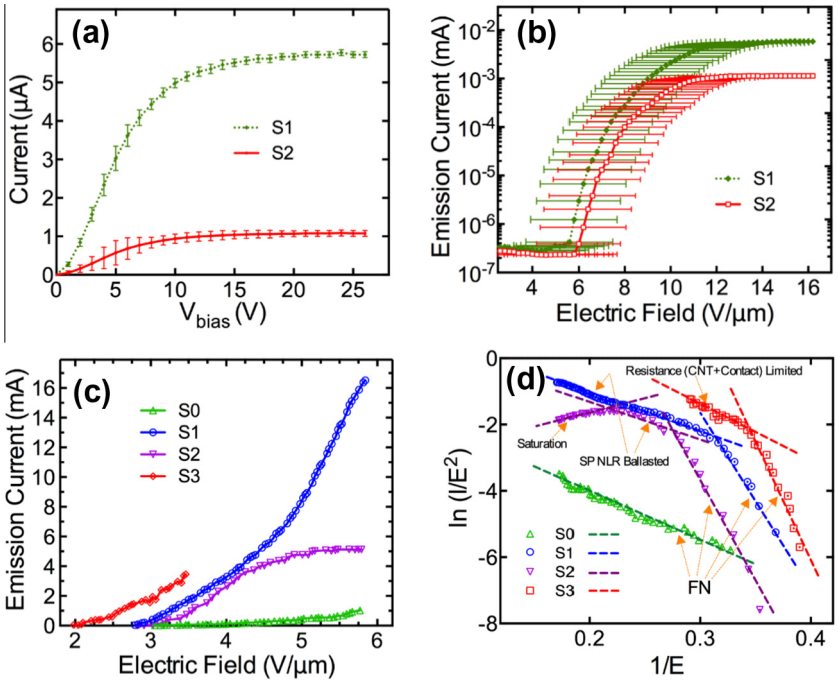

Fig. 4 – (a) The current–voltage characterization of individual SPs in both S1 and S2, of which the saturation currents were ~5.6 μA and ~1.1 μA, respectively. The error bars represent the performance variation of SPs. (b) Field emission *I–E* curves of a single CNT–SP emitter in S1 and S2, which also saturated to ~5.6 μA and ~1.1 μA, respectively. The error bars show the variation of driving field of emitters. (c) Field emission *I–E* curves of FEAs (area of 1 mm^2, containing 4900 emitter units). Total emission currents of 1.1 mA (S0), 16.5 mA (S1), 5.16 mA (S2), and 3.4 mA (S3) were obtained. (d) FN curves of the FEAs, in which the difference emission regions were marked (FN: pure field emission region, SP NLR Ballasted: field emission ballasted by SP non-linear resistor, Resistance (CNT + Contact) limited: field emission limited by the resistance of CNTs and contact resistance between CNTs and SPs). (A color version of this figure can be viewed online.)

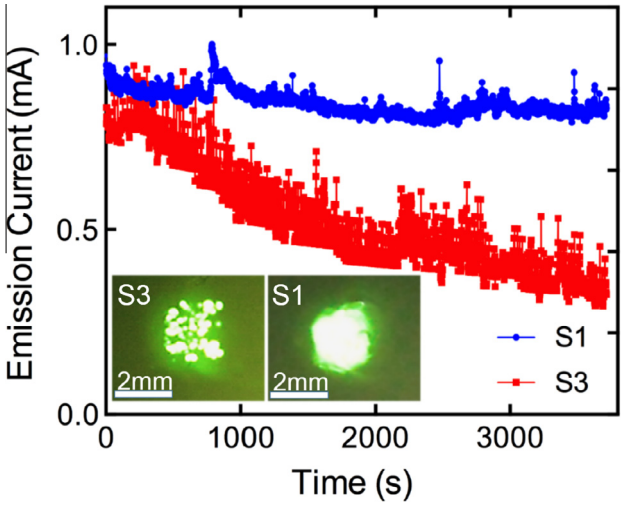

Fig. 5 – FE stability measurements of ballasted FEA (S1) over 60 min, showing an much more stable and undegraded emission, compared with unballasted FEA (S3). The inset shows the uniform field emission of S1 and S3 (approx. 2 × 2 mm^2) at an extraction field of 2 V/μm. (A color version of this figure can be viewed online.)

be attributed to protective effect of the SP NLR saturation current. The FE images (ZnO:Zn phosphor) of samples (S1 and S3) with a array area of 2 × 2 mm^2 were measured at an extraction field of 2 V/μm, as shown in the inset of Fig. 5. It is obvious that the FE uniformity of ballasted CNT array is much improved compared to that of unballasted CNT array.

3. Conclusion

We have developed high-current electron sources that achieve uniform emission using arrays of individually NLR ballasted CNT cluster emitters. Each emitter is fabricated on top of a vertical SP NLR. Compared with CNT cluster arrays on flat substrates, the driving field is greatly reduced due to the high aspect ratio of the CNT cluster combined with SPs. The *I–E* curves for the single emitter and emitter arrays show that the emission current is limited by the ballasting NLRs. Emitted currents over 16.5 mA were produced from a 1 mm^2 emmiting area. This paper describes a systematic method that combines numerical simulation and micro-probe testing to construct high performance field emission electron sources for future vacuum device applications.

4. Experimental section

4.1. *CNT array growth*

Vertically-aligned arrays of CNTs were grown on a heavily-doped n-type silicon chip via CVD. First, photolithography

was used to pattern the silicon substrate with 3 μm-wide square dots at a spacing of 15 μm, into which an Al (10 nm)/Fe (1 nm) multilayer catalyst was deposited by sputtering. The substrate was then heated to 700 °C at a pressure of 10^{-2} mbar. During heating, ammonia gas was introduced in order to etch the surface of the iron catalyst islands. Acetylene was used as the carbon source, and was introduced to the deposition chamber once the temperature had reached 750 °C. The growth process lasted for 5 min, yielding CNTs of nearly 5 μm in height.

4.2. *Field emission testing of single emitter unit*

The field emission measurements on single CNT cluster and single CNT–SP were performed in a SEM chamber equipped with a nano-manipulator, which was fixed with a cleaned tungsten tip with a radius of 800 nm as the anode probe. In the experiments, the distance between the anode probe and the top of emitter was set to ~600 nm. A picoammeter with a power supply (Keithley 2400) was employed to record the field emission current. The typical vacuum chamber pressure was $\sim 8 \times 10^{-5}$ Pa. Field emission measurements were performed cluster to cluster in the array.

4.3. *Field emission testing of FEA*

We loaded the CNT–SP array into an ultra-high vacuum (UHV) chamber with a base pressure of 10^{-9} Torr. The sample was heated to 200 °C for 24 h to eliminate water vapor or other possible residual adsorbates. The distance between anode and cathode was 250 μm defined using ceramic spacers. The n-type silicon substrate was connected to ground through an ohmic contact. The anode was driven positively using a variable DC voltage power supply. The emitted electrons were measured as anode current by a Keithley 485 picoammeter.

4.4. *Characterization*

Surface morphologies were characterized using scanning electron microscopy (SEM, Hitachi, S-4800) and high-resolution transmission electron microscopy (HRTEM JEOL-2010F). Raman analysis was performed using a micro-Raman microscope (Horiba JobinYvon, LabRAM HR800).

Acknowledgements

This work is supported by National Natural Science Foundation of China (11427808 and 51202027) and China Postdoctoral Science Foundation (2014M550676).

Appendix A. Supplementary data

Supplementary data associated with this article can be found, in the online version, at http://dx.doi.org/10.1016/j.carbon.2015.03.018.

REFERENCES

[1] Liu P, Wei Y, Liu K, Liu L, Jiang KL, Fan SS. New-type planar field emission display with super aligned carbon nanotube yarn emitter. Nano Lett 2012;12:2391–6.
[2] Kronhaus I, Kapulkin A, Guelman M. Field emission cathode with electron optics for use in Hall thrusters. J Appl Phys 2010;108. 054507-1-8.
[3] Gidcumb E, Gao B, Shan J, Inscoe C, Lu JP, Zhou O. Carbon nanotube electron field emitters for X-ray imaging of human breast cancer. Nanotechnology 2014;25. 245704-1-10.
[4] Jeong JW, Kim JW, Kang JT, Choi S, Ahn S, Song YH. A vacuum-sealed compact X-ray tube based on focused carbon nanotube field-emission electrons. Nanotechnology 2013;24. 085201-1-8.
[5] Whaley DR, Duggal R, Armstrong CM, Bellew CL, Holland CE, Spindt CA. 100 W operation of a cold cathode TWT. IEEE Trans Electron Devices 2009;56:896–904.
[6] Teo KBK, Minoux E, Hudanski L, Peauger F, Schnell JP, Gangloff L, et al. Microwave devices – carbon nanotubes as cold cathodes. Nature 2005;437:968–9.
[7] Manohara HM, Toda R, Lin RH, Liao A, Bronikowski MJ, Siegel PH. Carbon nanotube bundle array cold cathodes for THz vacuum tube sources. J Infrared Millimeter Terahertz Waves 2009;30:1338–50.
[8] Pandey A, Prasad A, Moscatello JP, Engelhard M, Wang CM, Yap YK. Very stable electron field emission from strontium titanate coated carbon nanotube matrices with low emission thresholds. ACS Nano 2013;7:117–25.
[9] Sun YH, Yeow JTW, Jaffray DA. Design and fabrication of carbon nanotube field-emission cathode with coaxial gate and ballast resistor. Small 2013;9:3385–9.
[10] Sridhar S, Tiwary C, Vinod S, Taha-Tijerina JJ, Sridhar S, Kalaga K, et al. Field emission with ultra low turn on voltage from metal decorated carbon nanotubes. ACS Nano 2014;8:7763–70.
[11] Navitski A, Muller G, Sakharuk V, Prudnikava AL, Shulitski BG, Labunov VA. Efficient high-current field emission from arrays of carbon nanotube columns. J Vac Sci Technol B 2010;28. C2B14–19.
[12] Kakade BA, Pillai VK, Late DJ, Chavan PG, Sheini FJ, More MA, et al. High current density, low threshold field emission from functionalized carbon nanotube bucky paper. Appl Phys Lett 2010;97. 073102-1-3.
[13] Sameera I, Bhatia R, Prasad V, Menon R. High emission currents and low threshold fields in multi-wall carbon nanotube-polymer composites in the vertical configuration. J Appl Phys 2012;111. 044307-1-5.
[14] Lee H, Goak J, Choi J, Kong B, Lee CH, Kim KB, et al. High-current field emission of point-type carbon nanotube emitters on Ni-coated metal wires. Carbon 2012;50:2126–33.
[15] Lahiri I, Wong J, Zhou ZL, Choi WB. Ultra-high current density carbon nanotube field emitter structure on three-dimensional micro-channeled copper. Appl Phys Lett 2012;101. 063110-1-3.
[16] Wang QL, Cui YK, Di YS, Li C, Chen XQ, Zhang XB, et al. Very large cathode current and long term stability of vacuum sealed tubes with engrafted-carbon-nanotube emitters. Diam Relat Mater 2014;47:40–5.
[17] Yoon DH, Choi YC. Improved field emission stability and uniformity of printed carbon nanotubes prepared using high energy-milled glass frit. Curr Appl Phys 2013;13:1477–81.
[18] Dall'Agnol F, Engelsen D. Nanoscale Res Lett 2013;8:319–24.
[19] She JC, Xu NS, Deng SZ, Chen J, Bishop H, Huq SE, et al. Vacuum breakdown of carbon-nanotube field emitters on a silicon tip. Appl Phys Lett 2003;83:2671–3.

[20] Minoux E, Groening O, Teo KBK, Dalal SH, Gangloff L, Schnell JP, et al. Achieving high-current carbon nanotube emitters. Nano Lett 2005;5:2135–8.
[21] Gangloff L, Minoux E, Teo KBK, Vincent P, Semet VT, Binh VT, et al. Self-aligned, gated arrays of individual nanotube and nanowire emitters. Nano Lett 2004;4:1575–9.
[22] Milne WI, Teo KBK, Chhowalla M, Arnaratunga GAJ, Pribat D, Legagneux P, et al. Aligned carbon nanotubes/fibers for applications in vacuum microwave devices. Curr Appl Phys 2002;2:509–13.
[23] Zhang G, Chen J, Deng SZ, She JC, Xu NS. Damages of screen-printed carbon nanotube cold cathode during the field emission process. Ultramicroscopy 2009;109:385–9.
[24] Liang XH, Deng SZ, Xu NS, Chen J, Huang NY, She JC. On achieving better uniform carbon nanotube field emission by electrical treatment and the underlying mechanism. Appl Phys Lett 2006;88. 111501-1-3.
[25] Li C, Zhang Y, Cole MT, Shivareddy SG, Barnard JS, Lei W, et al. Hot electron field emission via individually transistor-ballasted carbon nanotube arrays. ACS Nano 2012;6:3236–46.
[26] Swanwick ME, Keathley PD, Fallahi A, Krogen PR, Laurent G, Moses J. Nanostructured ultrafast silicon-tip optical field-emitter arrays. Nano Lett 2014;14:5035–43.
[27] Baker FS, Williams J, Osborn AR. Field-emission from carbon fibers – new electron source. Nature 1972;239:96–8.
[28] Lee MJG. Field-emission of hot-electrons from tungsten. Phys Rev Lett 1973;30:1193–6.